crystals

MDPI

Article

Vacuum-Filtration-Assisted Ice-Templated Freeze Drying for Preparing Capacitive Graphene Aerogel for Thermal Management

Yuze Xing [1,2], Hui Jia [1], Zhefan Wang [1,2], Lijing Xie [1], Dong Liu [1,2], Zheng Wang [1,2], Meng Li [1,2] and Qingqiang Kong [1,*]

[1] CAS Key Laboratory of Carbon Materials, Institute of Coal Chemistry, Chinese Academy of Sciences, Taiyuan 030001, China
[2] University of Chinese Academy of Sciences, Beijing 100049, China
* Correspondence: kongqq@sxicc.ac.cn

Abstract: Graphene aerogel (GA) is widely used in electronic devices owing to its light weight, elasticity, and excellent thermal conductivity. GA has been prepared using various methods. However, the preparation process is complex and the thickness is hard to control, which limits its application. There is an urgent need for a new and simple method to fabricate graphene aerogel. Herein, we describe a novel strategy for fabricating GA via a vacuum filtration–ice template freeze-drying method. The stability of graphene oxide slurry (GOS) was changed by using hydrochloric acid (HCl, 0.12 mol/L), and then GA was quickly obtained by vacuum filtration–ice template freeze drying and graphitization. The obtained GA reveals a symmetrical hyperbolic structure in the vertical direction, giving it excellent thermal and electrical conductivity and good compression performance. The electrical conductivity is up to 14.87 S/cm and the thermal conductivity is 1.29 W m^{-1} K^{-1} when the density is 36 mg cm^{-3}. The pressure only needs 0.013 MPa when the strain of GA is 50%. GA has considerable potential for the application of supercapacitors owing to the high conductivity and low density.

Keywords: graphene aerogel; vacuum filtration–ice template method; thermal conductivity; supercapacitor

check for updates

Citation: Xing, Y.; Jia, H.; Wang, Z.; Xie, L.; Liu, D.; Wang, Z.; Li, M.; Kong, Q. Vacuum-Filtration-Assisted Ice-Templated Freeze Drying for Preparing Capacitive Graphene Aerogel for Thermal Management. *Crystals* **2023**, *13*, 458. https://doi.org/10.3390/cryst13030458

Academic Editor: Rajratan Basu

Received: 15 February 2023
Revised: 26 February 2023
Accepted: 28 February 2023
Published: 7 March 2023

Copyright: © 2023 by the authors. Licensee MDPI, Basel, Switzerland. This article is an open access article distributed under the terms and conditions of the Creative Commons Attribution (CC BY) license (https://creativecommons.org/licenses/by/4.0/).

1. Introduction

Energy issues are a common concern around the world, so reducing unnecessary energy consumption and releasing excess heat from equipment have become an important focus of scientific research. With the rapid increase in energy consumption in the construction field, the demand for appropriate technologies to improve the thermal performance of buildings is also growing. Meanwhile, with the rapid development of information technology, the equipment is developing towards integration, miniaturization, and high frequency, which also leads to the emergence of local hot spots inside the equipment due to the inability to dissipate a large amount of heat. According to past research, phase change materials can improve the demand for thermal energy storage in buildings and are potential thermal energy storage media [1,2], and thermal interface materials are used to solve heat dissipation issues. Graphene can be constructed into three-dimensional materials for energy storage and energy conversion due to its excellent thermal conductivity, electrical conductivity, and mechanical performance [3,4]. Graphene-based macroscopic materials include graphene film [5], graphene aerogel [6], graphene foam [7], and vertical graphene [8]. GA with a three-dimensional structure has been studied and applied to supercapacitors [9], sensors [10], thermal interface materials [6], and phase change materials [11]. GA was prepared using various methods; for example, the hydrothermal reduction method [11], the ice template method [12], chemical vapor deposition (CVD) [13], and 3D printing [14].

In recent years, there have been many articles reporting the preparation methods of GA. Graphene/multi-walled carbon nanotube (MWCNT) aerogel was fabricated through hydrothermal reduction and high-temperature annealing at 2800 °C. The graphene/MWCNTs aerogels have a continuous vertical structure. After compounding with silicone rubber, the maximum thermal conductivity reaches 1.3 W m^{-1} K^{-1} [15]. Nevertheless, the hydrothermal reduction method at 180 °C needs significant amounts of energy. Super-elastic GA with three-dimensional networks was fabricated by ice template. It could be compressed at 80% strain and maintain structural integrity [6]. Super-elastic and durable GA was produced by melamine foam. The GA possessed excellent elasticity with a compressive strain of 95% [10]. In addition, the resulting GA could be used in pressure/strain sensors due to its stable current response. Worsley [14] and co-workers fabricated three-dimensional highly compressible graphene aerogel with light weight and highly conductive properties via 3D printing. The GA shows a compressive strain of 90%. However, these reports on the preparation of GA are complex and have high energy consumption. A new method with simple preparation and low energy consumption for preparing GA needs to be developed.

Herein, we describe a novel strategy to fabricate GA using a vacuum filtration–ice template freeze-drying method. The stability of GOS with different concentrations of HCl was investigated by using atomic force microscopy and a zeta analyzer. The appropriate hydrochloric acid concentration was determined by analyzing the zeta potential value and the viscosity of GOS. Graphene oxide hydrogel was quickly obtained by vacuum filtration after the stability of GOS was destroyed. GA was obtained by ice template freeze-drying and graphitization at 2800 °C. The application of this method provides a new three-dimensional symmetrical hyperbolic structure. Therefore, the obtained GA possesses excellent thermal and electric conductivity, as well as good compressibility. GA can be further applied to thermal interface materials (TIMs) for electronic devices, phase change materials (PCMs) for energy storage, and sensors for detecting human health. This article provides a new strategy for large-scale preparation and broad practical application prospects of GA with a new structure.

2. Experiments

2.1. Materials

Graphene oxide slurry was fabricated by a modified Hummers' method in our past research [3,16,17]. Hydrochloric acid (36–38%, AR, 12 mol/L) was purchased from Greagent (Shanghai, China).

2.2. Preparation of GOS Treated with Different Concentrations of HCl

HCl solutions with concentrations of 12 mol/L, 1.2 mol/L, 0.12 mol/L, and 0.012 mol/L were prepared by using HCl (12 mol/L) and deionized water; 1 mL GOS (2 mg/mL) and 9 mL HCl solution (12 mol/L, 1.2 mol/L, 0.12 mol/L, 0.012 mol/L) were mixed to obtain a mixed solution. The mixed solutions were labeled as GO/HCl-12, GO/HCl-1.2, GO/HCl-0.12, and GO/HCl-0.012; 1 mL GOS (2 mg/mL) and 9 mL deionized water were mixed as a comparison sample, which was named GO/HCl-0.

2.3. Preparation of GA

Firstly, GOS (2 mg/mL, 100 mL) and HCl (0.12 mol/L, 2 mL) were mixed to obtain the resulting mixed solution. The mixed solution was stirred at room temperature for half an hour. Secondly, graphene oxide hydrogel was rapidly prepared via vacuum filtration, and then graphene oxide aerogel was obtained using ice template freeze drying. Thirdly, the above graphene oxide aerogel was placed into a tube furnace for high-temperature heat treatment in an Ar atmosphere. The specific heating process is as follows: First, the temperature of the tube furnace was increased from room temperature to 100 °C at 5 °C min^{-1}. Second, the temperature was increased from 100 °C to 200 °C at 1 °C min^{-1} to avoid producing a large amount of gas due to the removal of oxygen-containing functional groups of graphene oxide during the heating process. Third, the temperature was increased from

200 °C to 700 °C at 5 °C min^{-1} and kept constant for two hours. Fourthly, the obtained aerogel was put into the graphitization furnace in an Ar atmosphere for graphitization treatment. The graphitization process is as follows: The temperature of the graphitization furnace was increased from room temperature to 2800 °C at 10 °C min^{-1} and kept constant for two hours. The GA was obtained after the above steps.

2.4. Characterization

The zeta potential was explored using a zeta potential analyzer (Zetasizer Nano ZS90, Malvern, Britain). Atomic force microscopy (Innova, Bruker, Berlin, Germany) was applied to assess the size and shape of graphene oxide sheets treated with different concentrations of HCl. Viscosity is measured by a viscosity tester (MSK-SFM-VT, MTI, Zhengzhou, China). The micromorphology of GA and graphene oxide sheets was analyzed by a scanning electron microscope (Phenom Prox, Phenom Scientific, Eindhoven, The Netherlands). Crystallinity information on GA was obtained by X-ray diffraction (XtaLAB mini^{TM} II, Rigaku, Tokyo, Japan). The defect information of GA was studied by Raman spectra (LabRAM HR Evolution, Horiba, Kyoto, Japan). The thermal conductivity of GA was assessed using the standard of the American Society for Testing and Materials (ASTM) D5470. The compressive property was tested using electromechanical universal testing machines (Instron 5969, Instron, Norwood, MA, USA). The electrical conductivity was investigated by four-probe conductivity equipment. An infrared thermal imager (USA, Fluke Ti32) was utilized to observe and record the IR images. Cyclic voltammetry (CV) was tested through VMP3 Booster (Bio-logic SAS, Seyssinet-Pariset, France). Electrochemical impedance spectroscopy and galvanostatic charge–discharge (GCD) measurements were measured using the Autolab workstation (PGSTSAT 302 N, Metrohm, Herisau, Switzerland). The cycle stability was evaluated on Land CT2001A battery tester (LAND, Shanghai, China) at 2.7 V.

3. Results and Discussion

3.1. Morphology of GOS

A macroscopic photograph of GOS treated with different concentrations of HCl is shown in Figure 1. This image was taken within half an hour of sample preparation. As a strong electrolyte, HCl can ionize H^+ ions with positive charge in aqueous solution. Graphene oxide is negatively charged. Since graphene oxide can be uniformly dispersed in aqueous solution and the diameter of the graphene oxide sheet is greater than 1 μm, GOS can be regarded as a colloidal solution. Therefore, the stability of the GOS is destroyed after the H^+ ions with positive charge are added to the GOS and the stability gradually deteriorates with the increment in electrolyte concentration. The GOS changes from a stable to an unstable state with the increment in HCl concentration. When the HCl concentration is 1.2 mol/L and 12 mol/L, the GOS becomes unstable with the agglomeration of GOS. When the concentration of HCl is 0.12 mol/L and 0.012 mol/L, the macroscopic state of the GOS is not different from that of the contrast sample. The above results show that the GOS can maintain a stable state as the concentration of HCl is 0.12 mol/L.

To further study the microscopic morphology of GOS treated with different concentrations of HCl, the AFM was used to investigate the thickness and shape of the GO sheets (Figure 2a–e). The thickness of pure graphene oxide sheets (2 mg/mL) is 10–13 nm, indicating that graphene oxide sheets are stacked by multilayer graphene [16]. The GOS exhibits light-brown coloration, which illustrates good dispersion of GOS (Figure 2a). In Figure 2b, the AFM image of GO/HCl-0.012 shows that the physical diameter of graphene oxide sheets is 31–35 nm and the graphene oxide sheets tend to aggregate. The above phenomena show that the addition of HCl will decrease the electrostatic repulsion between graphene oxide sheets and enhance the degree of charge screening [18]. The graphene oxide sheet layer and the agglomerated state co-exist in GO/HCl-0.12, and the thickness of graphene oxide sheets becomes larger (39–145 nm), indicating that the GOS is in a metastable state (Figure 2c). The thickness of graphene oxide sheets continues to increase as the concentration of HCl is 1.2 mol/L and 12 mol/L, which shows the occurrence of GOS coagulation

(Figure 2d,e). The results exhibit the negative charge of the graphene oxide sheet being gradually screened with the increase in HCl concentration, leading to a decrease in the potential energy contributed by electrostatic repulsion [19]. With the increase in HCl, the total energy barrier height decreases, and the stability of GOS becomes worse.

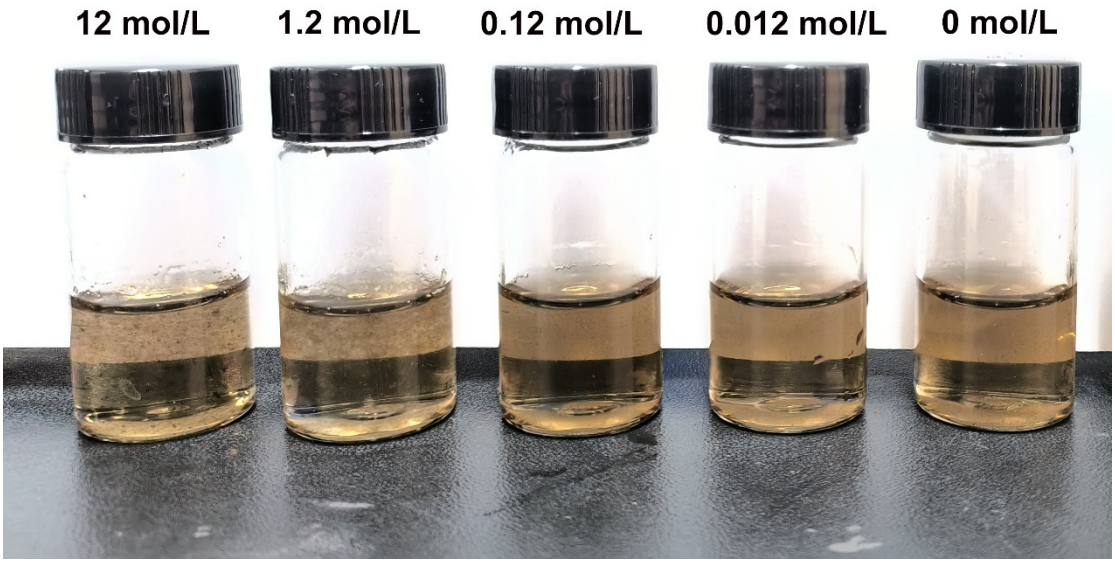


Figure 1. A macroscopic photograph of GOS treated with different concentrations of HCl (12 mol/L, 1.2 mol/L, 0.12 mol/L, 0.012 mol/L, 0 mol/L).

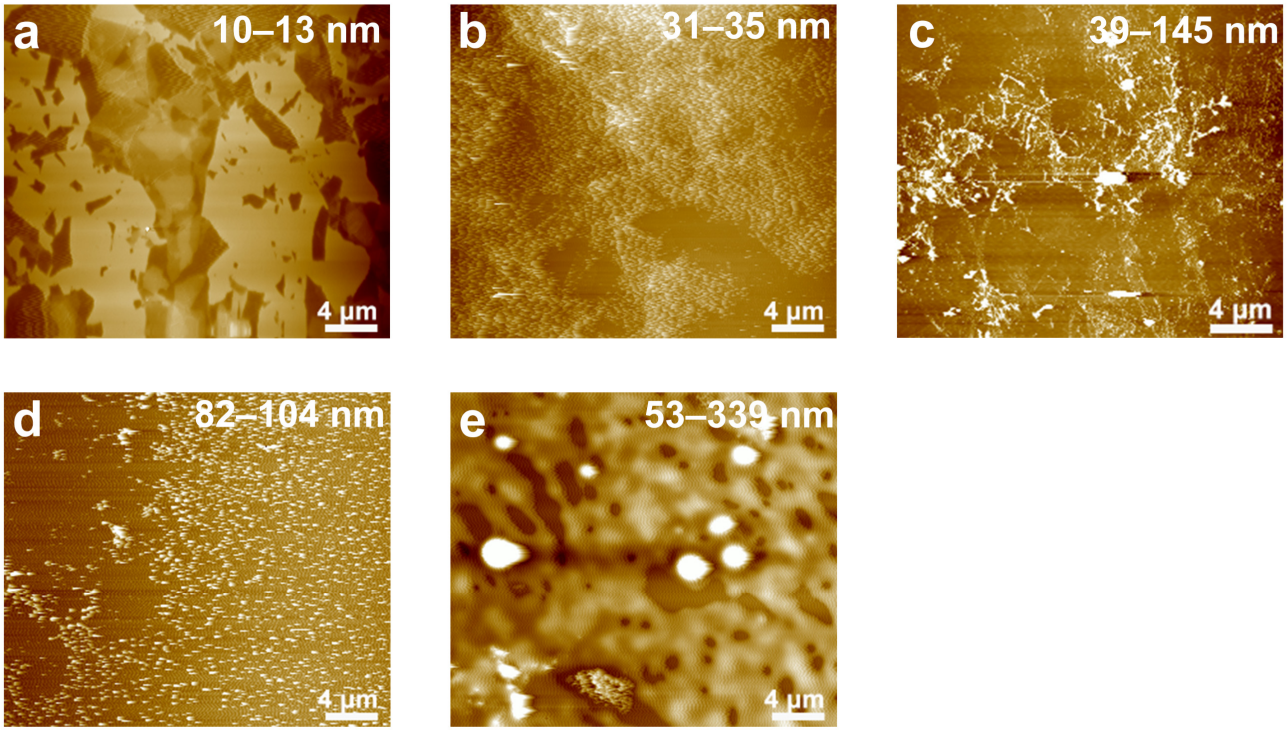


Figure 2. The AFM images of (**a**) GO/HCl-0, (**b**) GO/HCl-0.012, (**c**) GO/HCl-0.12, (**d**) GO/HCl-1.2, and (**e**) GO/HCl-12.

3.2. Properties of GOS

The viscosity of GOS is affected by the size and shape of graphene oxide particles. Therefore, the viscosity of GOS was studied to study the stability of GOS. The viscosity tester was used to further explore the viscosity of GOS treated with different hydrochloric

acid concentrations (Figure 3a). With the increase in HCl, the viscosity of GOS increases gradually from 23.96 Pa·s to 31.44 Pa·s. The asymmetry of graphene oxide particles causes an increase in the viscosity of graphene oxide with an increment in particles [20]. Zeta potential was utilized to further study the stability of GOS. As shown in Figure 3b, the potential value of GO/HCl-0 is −27.5 mV, showing good stability. In addition, the surface of graphene oxide particles in GO/HCl-0 is negatively charged according to the potential [21]. As the concentration of HCl increases to 0.12 mol/L, the absolute value of the potential of the GOS gradually decreases to 2.81 mV, indicating that the stability of the slurry becomes worse. The potential of GO/HCl-1.2 and GO/HCl-12 is 0.479 mV and 3.85 mV, which exhibits that the negative charge of graphene oxide is completely neutralized [22]. The GO/HCl-1.2 is unstable due to nearing the isoelectric point, which is also consistent with the macroscopic state of graphene oxide (Figure 1). Meanwhile, due to the increase in HCl, the charge of graphene oxide particles is screened, resulting in poor hydrophilicity of graphene oxide particles [23–25]. This result leads to a rapid removal of water from graphene oxide particles during vacuum filtration, accelerating the preparation process of graphene oxide hydrogel. Studying the GOS treated with different concentrations of hydrochloric acid shows GO/HCl-0.12 has relatively good stability and small viscosity. In addition, graphene oxide in GO/HCl-0.12 has a certain hydrophobicity compared with GO/HCl-0, which can quickly prepare graphene oxide hydrogel. Therefore, GO/HCl-0.12 is the most suitable precursor for the fabrication of GA.

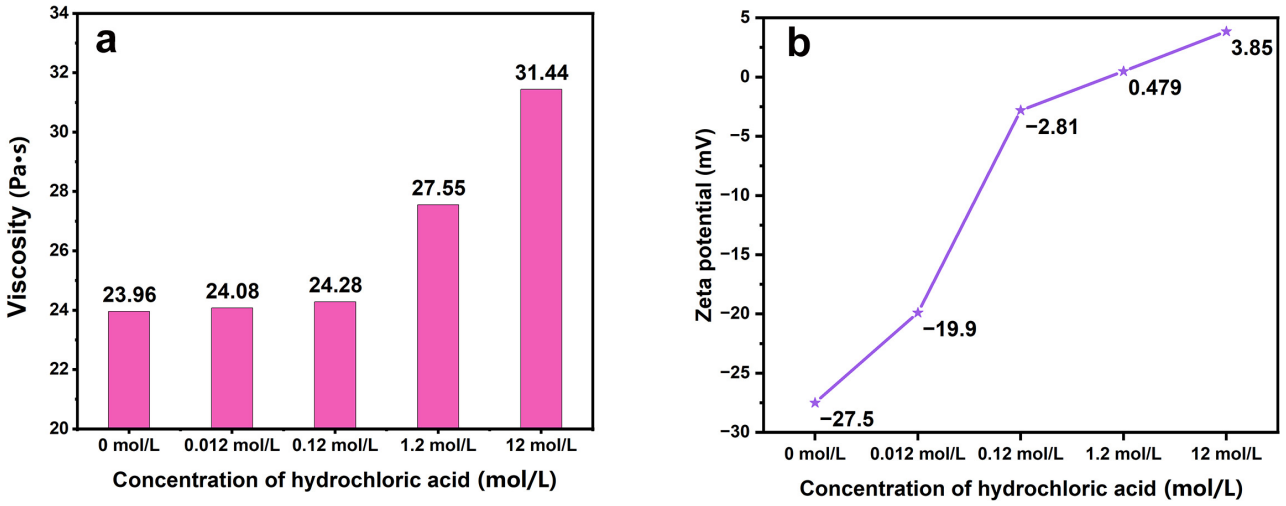


Figure 3. (**a**) Viscosity and (**b**) zeta potential of GOS treated with different concentrations of HCl.

3.3. Morphology and Structure of GA

GOS after HCl treatment at a concentration of 0.12 mol/L was used to fabricate GA by vacuum filtration–ice template freeze drying and the subsequent graphitization process. The above preparation method is a simple operation, low in cost, and with controllable thickness of GA. Therefore, the thickness of GA can be adjusted at any time according to practical application requirements. The photograph of the resulting GA is seen in Figure 4a. The planar SEM image of GA exhibits a flat surface similar to a graphene film, which is attributed to the stacking of graphene sheets affected by gravity during vacuum filtration (Figure 4b). Therefore, GA possesses the same in-plane heat spreader ability as graphene film. As shown in Figure 4c, the symmetrical hyperbolic structure is displayed in the vertical direction of GA because the graphene oxide hydrogel prepared by vacuum filtration grows in the vertical direction due to the influence of ice crystals during the ice template method. The symmetrical hyperbolic structure of GA can also increase the out-plane thermal conductivity. Owing to the symmetrical hyperbolic structure, GA has a large specific surface area, which can be used to provide more ion adsorption sites in the

field of supercapacitors [26]. Meanwhile, the three-dimensional network structure leads to excellent compression performance and elasticity of GA [6].

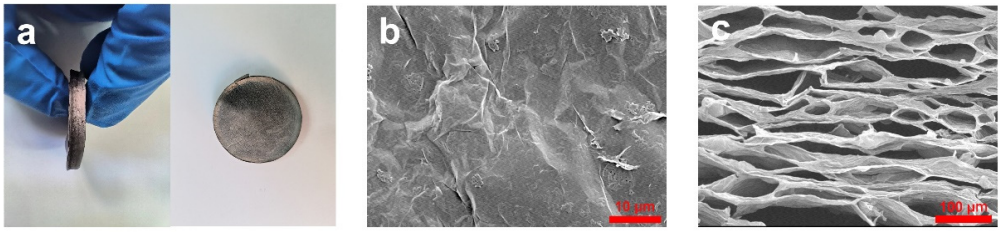


Figure 4. (**a**) Photograph of GA, (**b**) planar SEM image, and (**c**) cross-sectional image of GA.

The graphitization degree and defect information of GA were explored using XRD and Raman spectroscopy. Furthermore, by calculating the I_D/I_G from Raman results, the value of I_D/I_G represents the content of the defect [27,28]. From Figure 5a, the D peak almost disappears, and the intensity of the G peak is very strong. According to the fitting calculation, the value of I_D/I_G is 0.05, which suggests that the defects are almost eliminated after graphitization [29,30]. The elimination and repair of the defects are beneficial to the transport of phonons. The crystallite size (L_a) is calculated by the method of Cançado [16]. The crystallite size affects the thermal conductivity of graphene. This is attributed to heat transferred in graphene by phonons, and the mean free path of phonons is the average distance between the free motion of phonons between two scatterings. The crystallite size determines the boundary of graphene, which aggravates the scattering of phonons and is not conducive to phonon transport between graphene. The increase in crystallite size will reduce the grain boundary, weakening the phonon scattering. Therefore, the thermal conductivity increases with the increment in the crystallite size. The crystallite size of graphene increases and the defects decrease during the process of high-temperature graphitization. After graphitization, the crystallite size of graphene reached 384.49 nm. The XRD pattern is shown in Figure 5b, and the 2θc of the (002) plane is 26.46°. According to the Bragg equation, the corresponding interlayer d-spacing is 0.0336 nm, close to pure graphite [31]. The peak intensity of the (002) plane of graphite is very strong, indicating that the crystallinity of GA is high. The graphitization degree (G) of GA was further investigated by Mering–Maire [32,33]. The value of G is 87.2%, which shows that the stacking of graphene sheets tends to be ordered after high-temperature graphitization. The analysis of the structural information of the GA shows the GA prepared by this new method is not different from the GA reported in the past [34].

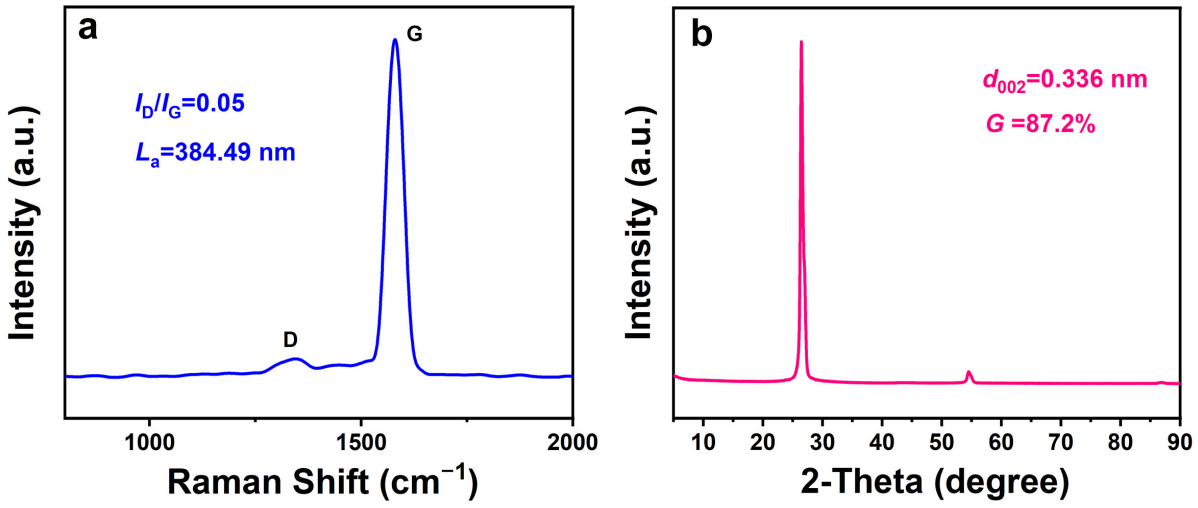


Figure 5. (**a**) Raman spectrum, (**b**) XRD patterns of GA.

3.4. Application of GA

The three-dimensional symmetric hyperbolic network structure in the vertical direction of GA provides the ability to quickly disperse the local high temperature on the surface while quickly transferring heat in the vertical direction. Therefore, GA possesses high thermal conductivity in the vertical direction, which can be applied to the field of thermal interface materials. To investigate the heat transfer capacity of GA, the thermal conductivity of GA at different pressures was measured (Figure 6a). As shown in Figure 6a, the thermal conductivity increases with the increment in pressure, and the maximum thermal conductivity is 1.29 W m^{-1} K^{-1} when the pressure is 398.5 KPa. This high thermal conductivity is owing to the increased density of GA during compression. Meanwhile, the application of pressure will also increase the connection between graphene and remove the air inside the aerogel. The thermal conductivity of some previously reported graphene-based composite materials is shown in Figure 6b. In past research, the preparation methods of GA were mainly the hydrothermal reduction method and ice template method. The GA fabricated by the above-mentioned method has a single structure and does not have a network structure, leading to the lack of a thermal conduction path in GA. GAs are usually used in a role of enhancing thermal conductivity in composite materials. Compared with previous studies, GA prepared by the vacuum filtration–ice template method had higher thermal conductivity. The result is attributed to the three-dimensional symmetric hyperbolic network structure, which provides more thermal conduction paths. In previous studies, GAs were mostly composited with polymer materials. In this paper, the internal voids of GA were filled with air, and the thermal conductivity of air is much lower than that of silicone rubber (SR) and polydimethylsiloxane (PDMS). However, the thermal conductivity of GA discussed in this paper is higher than that of graphene-based composites. The thermal conductivity is as high as 1.29 W m^{-1} K^{-1}. Therefore, it can be inferred that the GA discussed in this paper can better increase the thermal conductivity of polymer materials after compounding with polymer materials. The excellent thermal conductivity exhibits considerable potential for thermal interface materials.

To further study the heat transport performance in practical applications, the aerogel was heated on a 100 °C hot stage to observe the temperature change process and heating rate. The temperature of the upper surface of the aerogel at different times was recorded by the infrared images (Figure 6d). It can be clearly observed that the temperature of the aerogel rises rapidly to 33.9 °C at the moment of placement on the hot stage. The upper surface temperature of GA only requires 2 s to reach 62.7 °C from 33.9 °C, which shows an excellent heat transport performance.

Electrical conductivity is an important parameter for the practical application of GA. The electrical conductivity of some previously reported graphene-based composite materials is shown in Figure 6c; the electrical conductivity of GA in this paper is much higher than that of GA reported in the past. The high electrical conductivity of GA benefits from the complete lattice structure and the repair of the defect after graphitization. The electrical conductivity of GA is up to 14.87 S/cm. The result is attributed to the symmetrical hyperbolic structure of GA. The above results show that the GA prepared by the vacuum filtration–ice template method has excellent properties and broad application potential.

Carbon nanomaterials are often introduced into traditional refractory materials to improve thermal shock resistance and corrosion resistance, possessing high application value and application prospects. As shown in Figure 6e, the fire resistance of graphene aerogels was tested by directly burning them in the air. After burning at 500–600 °C for 10 s at the same position, the GA still maintains its original morphology, indicating that the GA can resist high temperature and fire. The above results are attributed to the graphitization of graphene aerogel, the complete elimination of defects, and the complete lattice structure. In addition, graphene has excellent thermal stability and chemical stability. Therefore, GA has a promising potential for the demand of the refractory material application.

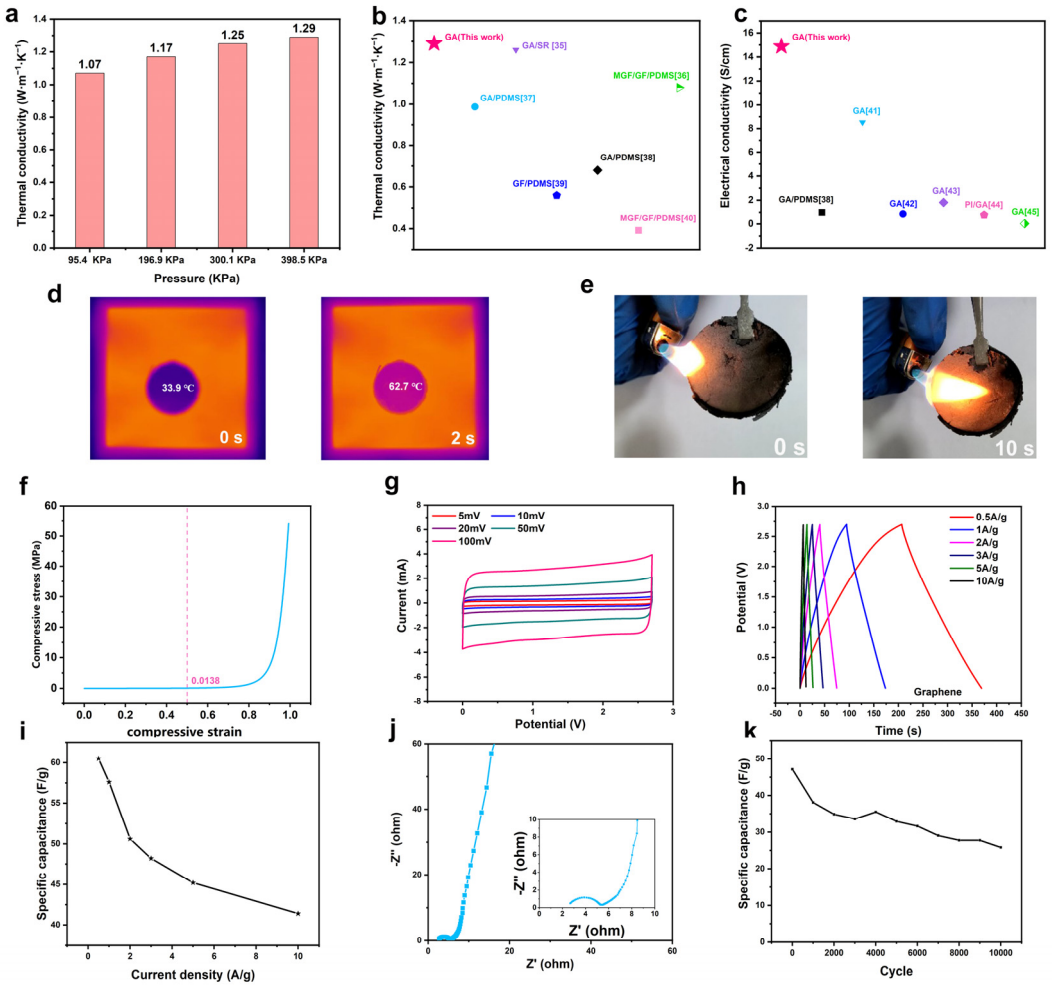


Figure 6. (**a**) Thermal conductivity of GA under different pressures, comparison of (**b**) thermal and (**c**) electrical conductivity of GA and other graphene-based materials in previous works [35–45]. (**d**) Infrared thermography images of GA heated for different times on a 100 °C hot stage, (**e**) fire resistance experiment of GA, (**f**) compressive of stress–strain of GA, (**g**) cyclic voltammetry curves with different scan rates, (**h**) galvanostatic charge/discharge curves with different current density, (**i**) capacitance retention with different currents density, (**j**) Nyquist plots, (**k**) cycling durability at 2.7 V.

A compression test was used to evaluate the compression properties of GA. GA has a good compression performance due to the internal three-dimensional network structure. Compared with the phenomenon reported in the past that GA is difficult to recover after pressure, the multilayer flat surface of the aerogel can buffer the pressure, and the vertical structure can support and bear the pressure; as a result, the GA can maintain good structural integrity after compression. In addition, the pressure required for GA to undergo 50% strain is only 0.013 MPa (Figure 6f), which gives it thermal management applications in integrated, lightweight electronic devices.

To study the application of GA in the field of supercapacitors, we first studied the electrochemical properties of graphene. As shown in Figure 6g,h, the CV curves of graphene exhibit a rectangular shape at 100 mV s^{-1}. In addition, the galvanostatic charge–discharge curve has almost no voltage drop, which further indicates that the material still possesses strong ion transport capacity. Figure 6i presents a good specific capacitance (61 F g^{-1}) at 0.5 A g^{-1}. To reveal the relationship between pore structure and ion diffusion kinetics, electrochemical impedance spectroscopy (EIS) was used to study the electrochemical properties of materials (Figure 6j). The material shows a small semicircle diameter in the

high-frequency region and a large linear slope in the low-frequency region, indicating that the material has fast ion transport ability and smaller charge transfer resistance, which is mainly caused by the high conductivity and highly crosslinked pore structure of the material. In Figure 6i, good electrochemical performance was demonstrated. At a current density of 1 A, the electrode has a capacity of nearly 28 F g^{-1} at 2.7 V after 10,000 cycles (Figure 6k). The above excellent electrochemical properties confirm the feasibility of graphene electrode operation under high-voltage windows. Therefore, GA has great potential for application as a supercapacitor.

4. Conclusions

A new preparation method for GA was developed. HCl, as a strong electrolyte, can ionize H^+ with positive charge in aqueous solution, which can change the stability of GOS. The vacuum filtration–ice template method was combined to fabricate GA using the GOS treated with 0.12 mol/L hydrochloric acid. The vacuum filtration method makes the GA have a flat surface, and the ice template method makes it possess a vertical structure. This new preparation method provides GA with a new three-dimensional symmetric hyperbolic network structure. After graphitization, the defects of GA were almost repaired, and the graphitization degree reached 87.2%. The crystallite size of graphene reached 384.49 nm. These features endow GA with excellent thermal conductivity, electrical conductivity, compressive properties, and fire resistance. The maximum thermal conductivity is 1.29 W m^{-1} K^{-1}. The electrical conductivity is 14.87 S/cm. The excellent performance of GA enables it to be applied in the fields of heat dissipation and sensors. In addition, the GA maintains its original structural integrity under burning for 10 s. Studying the electrochemical properties of graphene shows GA to have great potential in the field of supercapacitors. This paper provides a new method for preparing GA with a three-dimensional symmetrical hyperbolic structure, and the prepared GA has great application prospects in the thermal management of electronics, phase change materials, and sensors. At the same time, the introduction of electrolytes into GOS to prepare graphene-based materials with excellent properties also opens a door for the preparation of graphene-based materials with new structures.

Author Contributions: Conceptualization, Q.K. and H.J.; methodology, Y.X., D.L., Z.W. (Zheng Wang) and M.L.; data curation, Y.X. and Z.W. (Zhefan Wang); writing—review and editing, Y.X. and L.X. All authors have read and agreed to the published version of the manuscript.

Funding: This research was supported by the National Natural Science Foundation of China (52202055), the Joint Fund Project of Yulin University-Dalian National Laboratory for Clean Energy (Grant YLU-DNL Fund 2021009), and the Scientific and Technological Key Project of Shanxi Province (202101040201005).

Data Availability Statement: Data underlying the results presented in this paper are not publicly available at this time but may be obtained from the authors on reasonable request.

Conflicts of Interest: The authors declare no conflict of interest.

References

1. Ermiş, K.; Findik, F. Thermal energy storage. *Sustain. Eng. Innov.* **2020**, *2*, 66–88. [CrossRef]
2. Durakovic, B.; Mesetovic, S. Thermal performances of glazed energy storage systems with various storage materials: An experimental study. *Sustain. Cities Soc.* **2019**, *45*, 422–430. [CrossRef]
3. Chen, C.; Yang, Q.-H.; Yang, Y.; Lv, W.; Wen, Y.; Hou, P.-X.; Wang, M.; Cheng, H.-M. Self-Assembled Free-Standing Graphite Oxide Membrane. *Adv. Mater.* **2009**, *21*, 3541. [CrossRef]
4. Balandin, A.A.; Ghosh, S.; Bao, W.; Calizo, I.; Teweldebrhan, D.; Miao, F.; Lau, C.N. Superior thermal conductivity of single-layer graphene. *Nano Lett.* **2008**, *8*, 902–907. [CrossRef]
5. Akbari, A.; Cunning, B.V.; Joshi, S.R.; Wang, C.; Camacho-Mojica, D.C.; Chatterjee, S.; Modepalli, V.; Cahoon, C.; Bielawski, C.W.; Bakharev, P.; et al. Highly Ordered and Dense Thermally Conductive Graphitic Films from a Graphene Oxide/Reduced Graphene Oxide Mixture. *Matter* **2020**, *2*, 1198–1206. [CrossRef]
6. Lv, P.; Tan, X.-W.; Yu, K.-H.; Zheng, R.-L.; Zheng, J.-J.; Wei, W. Super-elastic graphene/carbon nanotube aerogel: A novel thermal interface material with highly thermal transport properties. *Carbon* **2016**, *99*, 222–228. [CrossRef]

7. Zhang, X.; Yeung, K.K.; Gao, Z.; Li, J.; Sun, H.; Xu, H.; Zhang, K.; Zhang, M.; Chen, Z.; Yuen, M.M.F.; et al. Exceptional thermal interface properties of a three-dimensional graphene foam. *Carbon* **2014**, *66*, 201–209. [CrossRef]
8. Xu, S.; Wang, S.; Chen, Z.; Sun, Y.; Gao, Z.; Zhang, H.; Zhang, J. Electric-Field-Assisted Growth of Vertical Graphene Arrays and the Application in Thermal Interface Materials. *Adv. Funct. Mater.* **2020**, *30*, 2003302. [CrossRef]
9. Tang, X.; Xia, S.; Luo, Q.; Liu, J.; Gong, H.; Deng, Y.; Chen, X.; Shao, J. Hierarchically Porous Graphene Aerogels with Abundant Oxygenated Groups for High-Energy-Density Surpercapacitors. *Energy Fuels* **2022**, *36*, 14433–14441. [CrossRef]
10. Li, C.; Jiang, D.; Liang, H.; Huo, B.; Liu, C.; Yang, W.; Liu, J. Superelastic and Arbitrary-Shaped Graphene Aerogels with Sacrificial Skeleton of Melamine Foam for Varied Applications. *Adv. Funct. Mater.* **2018**, *28*, 1704674. [CrossRef]
11. Yang, J.; Li, X.; Han, S.; Yang, R.; Min, P.; Yu, Z.-Z. High-quality graphene aerogels for thermally conductive phase change composites with excellent shape stability. *J. Mater. Chem. A* **2018**, *6*, 5880–5886. [CrossRef]
12. Yang, H.; Zhang, T.; Jiang, M.; Duan, Y.; Zhang, J. Ambient pressure dried graphene aerogels with superelasticity and multifunctionality. *J. Mater. Chem. A* **2015**, *3*, 19268–19272. [CrossRef]
13. Yan, J.; Qi, G.-Q.; Bao, R.-Y.; Yi, K.; Li, M.; Peng, L.; Cai, Z.; Yang, M.-B.; Wei, D.; Yang, W. Hybridizing graphene aerogel into three-dimensional graphene foam for high-performance composite phase change materials. *Energy Storage Mater.* **2018**, *13*, 88–95. [CrossRef]
14. Zhu, C.; Han, T.Y.-J.; Duoss, E.B.; Golobic, A.M.; Kuntz, J.D.; Spadaccini, C.M.; Worsley, M.A. Highly compressible 3D periodic graphene aerogel microlattices. *Nat. Commun.* **2015**, *6*, 6962. [CrossRef]
15. Liu, D.; Kong, Q.-Q.; Jia, H.; Xie, L.-J.; Chen, J.; Tao, Z.; Wang, Z.; Jiang, D.; Chen, C.-M. Dual-functional 3D multi-wall carbon nanotubes/graphene/silicone rubber elastomer: Thermal management and electromagnetic interference shielding. *Carbon* **2021**, *183*, 216–224. [CrossRef]
16. Jia, H.; Kong, Q.-Q.; Yang, X.; Xie, L.-J.; Sun, G.-H.; Liang, L.-L.; Chen, J.-P.; Liu, D.; Guo, Q.-G.; Chen, C.-M. Dual-functional graphene/carbon nanotubes thick film: Bidirectional thermal dissipation and electromagnetic shielding. *Carbon* **2021**, *171*, 329–340. [CrossRef]
17. Song, N.-J.; Chen, C.-M.; Lu, C.; Liu, Z.; Kong, Q.-Q.; Cai, R. Thermally reduced graphene oxide films as flexible Lateral heat spreaders. *J. Mater. Chem. A* **2014**, *2*, 16563–16568. [CrossRef]
18. Szabo, T.; Maroni, P.; Szilagyi, I. Size-dependent aggregation of graphene oxide. *Carbon* **2020**, *160*, 145–155. [CrossRef]
19. Wang, H.; Hu, Y.H. Electrolyte-induced precipitation of graphene oxide in its aqueous solution. *J. Colloid Interface Sci.* **2013**, *391*, 21–27. [CrossRef]
20. Esfahani, M.R.; Languri, E.M.; Nunna, M.R. Effect of particle size and viscosity on thermal conductivity enhancement of graphene oxide nanofluid. *Int. Commun. Heat Mass Transfer* **2016**, *76*, 308–315. [CrossRef]
21. Kim, J.; Cote, L.J.; Kim, F.; Yuan, W.; Shull, K.R.; Huang, J. Graphene Oxide Sheets at Interfaces. *J. Am. Chem. Soc.* **2010**, *132*, 8180–8186. [CrossRef] [PubMed]
22. Wu, L.; Liu, L.; Gao, B.; Munoz-Carpena, R.; Zhang, M.; Chen, H.; Zhou, Z.; Wang, H. Aggregation Kinetics of Graphene Oxides in Aqueous Solutions: Experiments, Mechanisms, and Modeling. *Langmuir* **2013**, *29*, 15174–15181. [CrossRef]
23. Hu, X.; Yu, Y.; Hou, W.; Zhou, J.; Song, L. Effects of particle size and pH value on the hydrophilicity of graphene oxide. *Appl. Surf. Sci.* **2013**, *273*, 118–121. [CrossRef]
24. Shih, C.-J.; Lin, S.; Sharma, R.; Strano, M.S.; Blankschtein, D. Understanding the pH-Dependent Behavior of Graphene Oxide Aqueous Solutions: A Comparative Experimental and Molecular Dynamics Simulation Study. *Langmuir* **2012**, *28*, 235–241. [CrossRef]
25. Chen, K.L.; Elimelech, M. Relating Colloidal Stability of Fullerene (C-60) Nanoparticles to Nanoparticle Charge and Electrokinetic Properties. *Environ. Sci. Technol.* **2009**, *43*, 7270–7276. [CrossRef]
26. Xin, Z.; Li, W.; Fang, W.; He, X.; Zhao, L.; Chen, H.; Zhang, W.; Sun, Z. Enhanced specific surface area by hierarchical porous graphene aerogel/carbon foam for supercapacitor. *J. Nanopart. Res.* **2017**, *19*, 386. [CrossRef]
27. Lucchese, M.M.; Stavale, F.; Ferreira, E.H.M.; Vilani, C.; Moutinho, M.V.O.; Capaz, R.B.; Achete, C.A.; Jorio, A. Quantifying ion-induced defects and Raman relaxation length in graphene. *Carbon* **2010**, *48*, 1592–1597. [CrossRef]
28. Martins Ferreira, E.H.; Moutinho, M.V.O.; Stavale, F.; Lucchese, M.M.; Capaz, R.B.; Achete, C.A.; Jorio, A. Evolution of the Raman spectra from single-, few-, and many-layer graphene with increasing disorder. *Phys. Rev. B* **2010**, *82*, 125429. [CrossRef]
29. Cancado, L.G.; Jorio, A.; Martins Ferreira, E.H.; Stavale, F.; Achete, C.A.; Capaz, R.B.; Moutinho, M.V.O.; Lombardo, A.; Kulmala, T.S.; Ferrari, A.C. Quantifying Defects in Graphene via Raman Spectroscopy at Different Excitation Energies. *Nano Lett.* **2011**, *11*, 3190–3196. [CrossRef] [PubMed]
30. Zhong, J.-H.; Zhang, J.; Jin, X.; Liu, J.-Y.; Li, Q.; Li, M.-H.; Cai, W.; Wu, D.-Y.; Zhan, D.; Ren, B. Quantitative Correlation between Defect Density and Heterogeneous Electron Transfer Rate of Single Layer Graphene. *J. Am. Chem. Soc.* **2014**, *136*, 16609–16617. [CrossRef]
31. Bacon, G.E. The interlayer spacing of graphite. *Acta Cryst.* **1951**, *4*, 558–561. [CrossRef]
32. Zou, L.H.; Huang, B.Y.; Huang, Y.; Huang, Q.H.; Wang, C.A. An investigation of heterogeneity of the degree of graphitization in carbon-carbon composites. *Mater. Chem. Phys.* **2003**, *82*, 654–662. [CrossRef]
33. Franklin, R.E. The structure of graphitic carbons. *Acta Cryst.* **1951**, *4*, 253–261. [CrossRef]
34. Hu, K.; Szkopek, T.; Cerruti, M. Tuning the aggregation of graphene oxide dispersions to synthesize elastic, low density graphene aerogels. *J. Mater. Chem. A* **2017**, *5*, 23123–23130. [CrossRef]

35. Zhang, W.; Kong, Q.-Q.; Tao, Z.; Wei, J.; Xie, L.; Cui, X.; Chen, C.-M. 3D Thermally Cross-Linked Graphene Aerogel-Enhanced Silicone Rubber Elastomer as Thermal Interface Material. *Adv. Mater. Interfaces* **2019**, *6*, 1900147. [CrossRef]
36. Zhao, Y.-H.; Zhang, Y.-F.; Bai, S.-L. High thermal conductivity of flexible polymer composites due to synergistic effect of multilayer graphene flakes and graphene foam. *Compos. Part A-Appl. Sci. Manufaturing* **2016**, *85*, 148–155. [CrossRef]
37. Lin, Y.; Chen, J.; Dong, S.; Wu, G.; Jiang, P.; Huang, X. Wet-resilient graphene aerogel for thermal conductivity enhancement in polymer nanocomposites. *J. Mater. Sci. Technol.* **2021**, *83*, 219–227. [CrossRef]
38. Zhang, Q.; Xu, X.; Li, H.; Xiong, G.; Hu, H.; Fisher, T.S. Mechanically robust honeycomb graphene aerogel multifunctional polymer composites. *Carbon* **2015**, *93*, 659–670. [CrossRef]
39. Zhao, Y.-H.; Wu, Z.-K.; Bai, S.-L. Study on thermal properties of graphene foam/graphene sheets filled polymer composites. *Compos. Part A-Appl. Sci. Manufaturing* **2015**, *72*, 200–206. [CrossRef]
40. Kong, K.T.S.; Mariatti, M.; Rashid, A.A.; Busfield, J.J.C. Enhanced conductivity behavior of polydimethylsiloxane (PDMS) hybrid composites containing exfoliated graphite nanoplatelets and carbon nanotubes. *Compos. Part B-Eng.* **2014**, *58*, 457–462. [CrossRef]
41. dos Santos-Gomez, L.; Garcia, J.R.; Montes-Moran, M.A.; Angel Menendez, J.; Garcia-Granda, S.; Arenillas, A. Ultralight-Weight Graphene Aerogels with Extremely High Electrical Conductivity. *Small* **2021**, *17*, 2103407. [CrossRef]
42. Worsley, M.A.; Pauzauskie, P.J.; Olson, T.Y.; Biener, J.; Satcher, J.H., Jr.; Baumann, T.F. Synthesis of Graphene Aerogel with High Electrical Conductivity. *J. Am. Chem. Soc.* **2010**, *132*, 14067–14069. [CrossRef] [PubMed]
43. Li, C.-B.; Li, Y.-J.; Zhao, Q.; Luo, Y.; Yang, G.-Y.; Hu, Y.; Jiang, J.-J. Electromagnetic Interference Shielding of Graphene Aerogel with Layered Microstructure Fabricated via Mechanical Compression. *ACS Appl. Mater. Interfaces* **2020**, *12*, 30686–30694. [CrossRef] [PubMed]
44. Zhang, J.; Luo, S.; Ma, Y.; Li, R.; Jin, Y.; Qiu, L.; Zhang, W. Monolithic polyimine vitrimer/graphene aerogel composites. *Chin. Chem. Lett.* **2023**, *34*, 107363. [CrossRef]
45. Afroze, J.D.; Tong, L.; Abden, M.J.; Yuan, Z.; Chen, Y. Hierarchical honeycomb graphene aerogels reinforced by carbon nanotubes with multifunctional mechanical and electrical properties. *Carbon* **2021**, *175*, 312–321. [CrossRef]

Disclaimer/Publisher's Note: The statements, opinions and data contained in all publications are solely those of the individual author(s) and contributor(s) and not of MDPI and/or the editor(s). MDPI and/or the editor(s) disclaim responsibility for any injury to people or property resulting from any ideas, methods, instructions or products referred to in the content.